Structural control of collapse events inferred by self-potential mapping on the Piton de la Fournaise volcano (La Réunion Island) Journal of Volcanology and Geothermal Research 209-210: 9-18 (2012)

Structural control of collapse events inferred by self-potential mapping on the Piton de la Fournaise volcano (La Réunion Island).

S. Barde-Cabusson[1, 2]; A. Finizola[3]; A. Peltier[4]; M. Chaput[1,3]; N. Taquet[1,3] ; S. Dumont[1, 5]; Z. Duputel[5]; A. Guy[5]; L. Mathieu[1]; S. Saumet[1]; F. Sorbadère[1]; M. Vieille[5]

1. Laboratoire Magmas et Volcans, Univ. Blaise Pascal-CNRS-OPGC, 5 rue Kessler, 63038 Clermont-Ferrand, France

2. Now: Instituto de Ciencias de la Tierra Jaume Almera (CSIC Barcelona), Barcelona, Spain

3. Laboratoire GéoSciences Réunion, Université de la Réunion, Institut de Physique du Globe de Paris, Sorbonne Paris-Cité, UMR CNRS 7154, 15 avenue René Cassin, BP 97715 Saint-Denis cedex 9, La Réunion, France

4. Institut de Physique du Globe de Paris et Université Paris Diderot, Sorbonne Paris-Cité, UMR CNRS 7154 – Géologie des Systèmes Volcaniques, 1 rue Jussieu, 75238 Paris cedex 05, France.

5. Ecole et Observatoire des Sciences de la Terre, Université Louis Pasteur, Strasbourg, France

Corresponding author :

Stéphanie Barde-Cabusson – Instituto Jaume Almera, Spain; email : s.barde.cabusson@gmail.com

Intended for publication in Journal of Volcanology and Geothermal Research

Abstract

Field surveys were performed on the terminal cone of Piton de la Fournaise in 2006 and 2008 to precisely map the self potential (SP) signal and determine the zonation of the hydrothermal activity both on the flanks of the cone and in the summit area, including inside the Bory and Dolomieu craters. SP maps inside the craters have been performed 8 months before the 5-7 April 2007 caldera collapse. Zonations appear both at the scale of the cone and of the summit and allow new interpretation of the electrical signal distribution on the terminal cone of Piton de la Fournaise. Superimposed to the SP maxima linked to the rift-zones, several areas of SP maxima associated with collapse structures have been detected: (1) in the summit area, the Bory and Dolomieu craters show the strongest SP values with amplitudes exceeding 2 V with respect to the base of the cone, and with a sharp lateral variation to the East, corresponding to the inner boundary of the Dolomieu caldera, collapsed on 5-7 April 2007, and (2) in the paleo pit craters surrounding the summit which show amplitudes similar to the Dolomieu-Bory craters. The analysis of the variations of the signal with time evidences a modification of the fluid flow pattern with a higher associated SP signature to the east in 2008. We interpret the amplification of fluid flow to the east in 2008 as a consequence of the eastward motion of the eastern flank of the volcano during the April 2007 eruption. The acquisition of SP data during two periods separated by the April 2007 eruption turns out to be a good opportunity to correlate the SP signal to the Piton de la Fournaise structure and to its evolution in term of hydrothermal and eruptive activity.

1- Introduction

The Piton de la Fournaise volcano is located on La Reunion Island, in the Indian Ocean. It is one of the most active volcanoes in the world with a mean of 2 eruptions per year since 1998 (Peltier et al., 2009a). The central active cone is located inside a U-shape depression formed by the Enclos Fouqué/Grandes Pentes/Grand Brûlé, a major structure opened on the Indian Ocean (Fig. 1). The origin of this structure (collapse, sliding or combination of both processes) is still debated. In the past 4.5 ka, the eruptive activity usually took place inside this U-shape depression and only a few eruptions occurred beyond its limits (Bachèlery, 1981).

The summit of the terminal cone is characterized by the presence of two collapse craters: Bory and Dolomieu (Fig. 1). In the past 200 years, the Bory crater did not experience major volcanic or tectonic activity of its own (Lénat and Bachèlery, 1990). On the other hand, the Dolomieu crater morphology was ceaselessly reshaped by successive collapse and eruptive events. The Dolomieu crater was the result of the coalescence of several pit craters and, until April 2007, the crater floor was leveled by accumulated lava flows and projections emitted by summit eruptions (Lénat and Bachèlery, 1990). During the large April 2007 eruption, the Dolomieu crater was affected by a major collapse increasing its depth to 340 m (Michon et al., 2007a; Urai et al., 2007). Today, the eruptive activity is slowly refilling the crater.

On the Piton de la Fournaise volcano, multiple SP studies have already been carried out in the Enclos Fouqué structure, on the terminal cone (Lénat, 1987; Malengreau et al., 1994; Zlotnicki et. al, 1994; Michel and Zlotnicki, 1998) and/or on outlying areas of the massif (Boubekraoui and Aubert, 1999; Levieux, 2004; Lénat, 2007; Barde-Cabusson et al., 2009). Malengreau et al. (1994) and Michel and Zlotnicki (1998) produced self-potential

93 maps of the terminal cone and the surrounding areas (some are presented in Figure 2). They
94 evidenced the coincidence of high SP values (with respect to the surrounding areas) with the
95 three main eruptive axes of the volcano, i.e. the northern and southern rift zones and the
96 N120º rift zone, also well-known as a major structural orientation for the island (Bachèlery,
97 1981; Michon et al., 2009a; Fig. 1).

98 At a lower scale, Malengreau et al. (1994) attributed the SP maxima recorded in the
99 summit area to the hydrothermal activity around the magma reservoir. Lénat et al. (2000)
100 supported this hypothesis from the interpretation of direct current electrical and transient
101 electromagnetic soundings. The authors interpreted the low resistivity zones inside the cone
102 as altered rocks of the hydrothermal system. In their interpretation, hydrothermal fluid
103 circulation is thus implicated to explain both the SP positive peak and the low resistivity zone.

104 Even if these previous SP studies identified the main eruptive axes draining
105 hydrothermal fluids, data spacing and measurement distribution did not allow discriminating
106 in detail the smallest structures, especially at the summit, an area strongly affected by
107 fractures. However it is important regarding the recent evolution of the summit area to well
108 constrain the active structure controlling its eruptive activity and its collapses. So, we carried
109 out new detailed SP measurements in order to constrain more precisely the structural limits
110 and the active hydrothermal zones at different scales from the edifice (terminal cone) to the
111 summit, taking into account the previous hydrological models on Piton de la Fournaise (Join
112 et al., 2005).

113 This paper presents the results of a self-potential study employed in characterize the electric
114 signal on the Piton de la Fournaise terminal cone. The data is discussed to determine the
115 distribution of the hydrothermal activity and its relations with the structure and dynamics of
116 this volcano. We also discuss the data in relation with the April 2007 Dolomieu collapse.

117

2- Data acquisition and processing

Self-potential (SP) signals refer to quasi-static electrical potential anomalies, usually measured at the ground surface of the Earth, that are associated with the occurrence of source current densities existing at depth (Sill, 1983; Corwin, 1997). Various sources can generate a difference of potential, but on active volcanoes, the main source of SP anomalies is related to the flow of the groundwater (Massenet and Pham, 1985; Ishido et al., 1997; Bedrosian et al., 2007). In this case, self-potential signals is generated by the streaming potential effect, related to the flow of the pore water relative to the mineral grain framework in saturated (Overbeek, 1952; Nourbehecht, 1963) and unsaturated conditions (Revil and Cerepi, 2004; Linde et al., 2007). The fact that the SP signal is generally positive in the flow direction can be understood thanks to the electric double (or triple) layer theory describing the electrochemical interactions occurring at the interface between a mineral and the pore water (e.g. Revil, 2002 and references therein). In active volcanoes, pH of the hydrothermal system can range from low (~2) to high (>10) values. However, experimental results (Revil, 2002) generally gives pH in the range 5–8, and therefore the zeta potential is usually negative. The surface of silicate and alumino-silicates of volcanic rocks is negatively charged. The corresponding negative fixed surface charge is counterbalanced by a mobile charge in the so-called electrical diffuse layer. The diffuse layer has a net charge of opposite sign to the surface charge of the mineral to maintain a global electroneutrality in the system. The flow of pore water drags most of the mobile positive charges of the electrical diffuse layer in the flow direction, generating a positive electric self-potential at the ground surface. Most hydrothermal systems associated with active volcanoes evidence a large positive SP anomaly in the area where fluid flow is upwelling (e.g. Revil, 2002; Ishido, 2004; Lénat, 2007). However, it is important to note that in some cases rocks are positively charged in neutral pH conditions and that some

143 volcanoes showing geothermal activity on their flanks have shown no positive anomalies
144 associated (Aizawa, 2008; Aizawa et al., 2008; Hase et al., 2003; Guichet and Zuddas, 2003).
145 Therefore, in absence of laboratory experiments to measure the zeta potential of the rocks, the
146 classic interpretation of SP data (hydrothermal upwelling corresponding to positive SP zone)
147 constitutes only an assumption.

148 We acquired a dense dataset of 4621 self-potential measurements (SP) on the Piton de
149 la Fournaise volcano in July and August 2006, i.e. 8 months before the large April 2007
150 eruption and Dolomieu collapse. We repeated the summit SP mapping in May 2008, one year
151 after the Dolomieu collapse. The SP equipment consisted of a high-impedance voltmeter
152 (~10 Mohm), a pair of $Cu/CuSO_4$ non-polarizing electrodes and an insulated copper cable.
153 During the measurements, the reference and moving electrodes were switched every few
154 hundred meters in order to avoid the systematic error due to electrodes offset. We controlled
155 the contact between the electrodes through the ground by checking the electric resistance
156 before each measure point. As a rule of thumb, the electrical resistance between the two
157 electrodes should be always ten times smaller than the internal impedance of the voltmeter
158 (Corwin, 1997).

159 Data were acquired along 12 profiles crossing the entire terminal cone, a circular loop
160 around the base of the cone, and a loop around the summit craters with a regular spacing of
161 20 m (Fig. 3b). In addition, we performed a denser measurement network in the summit area
162 with 24 radial lines outside the craters with a 2 m spacing, 15 radial lines from the center of
163 the Dolomieu crater, 4 from the center of the Bory crater, and 2 circular profiles along the
164 craters inner walls with a 20 m spacing (Fig. 3a, c, d). The whole measurement network is
165 interconnected so that we applied a closure correction along the loops, in order to limit
166 cumulative errors. The order of magnitude of the closure correction is of a few tens of
167 millivolts. Usually the 0 mV reference for SP measurements is taken at the sea or a water

168 table as it provides a constant value in time. Given no such stable reference is available in the
169 studied area, we used the self-potential map of a former study to connect our dataset to the sea
170 (data from Levieux, 2004 and Lénat, 2007). The datasets were joined in at point X 364.709,
171 Y 7650.933 (UTM-WGS84, km), in a zone where the hydrothermal and eruptive activity is
172 scarce (black arrow on Figure 3b).
173
174 3- Data analysis
175 In this section, we first describe the results obtained from the wide-scale SP map of the
176 terminal cone of Piton de La Fournaise and, in a second time, we detail the repartition of the
177 anomalies in the summit area.
178
179 3.1- Self-Potential map of the terminal cone
180
181 The entire cone is characterized by negative self-potential values relative to the sea.
182 On a typical profile crossing an active volcanic cone, the SP variations are axis-symmetrical
183 and a radial cross-section generally displays a W-shape centered on the cone (e.g. Ishido et
184 al., 1997; Zlotnicki et al., 1998; Revil et al., 2003; Ishido, 2004; Finizola et al., 2004; Lénat,
185 2007). On the Piton de la Fournaise, the SP map of the terminal cone, which we will consider
186 as a reference pattern, shows a continuous increase of the SP values from the base of the cone
187 to the summit area (Fig. 3b). We found an average SP/elevation gradient of 1.3 mV/m
188 (ranging from 0.2 to 3.7 mV/m) along profiles on the flanks of the terminal cone; the average
189 gradient along the 24 radial profiles around the crater is of 7mV/m (ranging from 3.1 to 15
190 mV/m and with Profile 6 showing a gradient of -12.2 mV/m); for the Dolomieu and Bory
191 craters, the SP/elevation graph shows a quasi-vertical alignment of the points (Fig. 4). The
192 highest SP variation from the base of the cone to the craters is about 2.3 V. The northern,

193 southern, and eastern flanks are the seats of three main elongated radial anomalies compared
194 to the reference pattern (Fig. 3b).
195
196 A radial SP anomaly extends on the northern flank with a roughly N150º direction,
197 near the crater, shifting to a N10º direction in the lower part of the cone (Fig. 3b). The
198 southern flank is affected by a N25º similar radial anomaly. Each of these two elongated
199 anomalies is about 1 km large and defines a SP maximum of about 1V amplitude with respect
200 to the surrounding areas. Farther east and west from those main axes the SP anomalies vanish
201 progressively. They seem to extend on both sides of the summit area, in the north and in the
202 south, beyond the investigated area.
203
204 On the eastern flank of the cone, a more diffuse SP maximum, outlined by the SP
205 contour lines, highlights a significant anomalous zone (profile 19 and 21 on figure 3b). The
206 maximum SP value is about -1600 mV in the lower part of the cone (at an elevation of
207 1900 m), and higher in the crater vicinity. It means the anomaly is about 400 mV and 600 mV
208 lower than the maximum values registered on the northern and southern flanks respectively.
209
210 Figure 5 shows a good correlation between the location of the eruptive fissures since
211 1981 and the position of the SP maxima. In particular the most recent eruptive fissures are
212 located on the highest SP values and their repartition follows a very similar orientation than
213 that of the northern and southern rift zones. In the NNE direction, no SP maximum anomaly
214 appears, while eruptive fissures exist. However this direction is barely followed by dykes,
215 compared to the rift zones. Only 4 dykes affected this direction in 35 years (Peltier et al.,
216 2009a).
217

These three main elongated anomalies were already visible in 1992-1993 and also in 1981 but with a lower amplitude on the northern one (Fig. 2; Malengreau et al., 1994, Michel et Zlotnicki, 1998).

3.2- Detailed self-potential map of the summit area

3.2.1- Self-potential zonation along the crater boundaries

With a color scale adapted to the SP amplitude of the summit area, interesting information appears about the SP signal zonation (Fig. 3a and 3c). The strongest anomalies are centered on the Bory and Dolomieu craters. A significant SP difference of up to several hundred millivolts exists between the crater floor and the rims of these two craters, except (1) on the northern border, close to profiles 3-4, (2) on the northwestern border, on profile 7, and (3) on the southeastern border, between profiles 15 and 21. For instance, in the northeastern side of Dolomieu, we observe a difference of approximately 600 mV between the rim and the Dolomieu crater floor. The usual hydrogeological gradients observed on the inactive flanks of Piton de la Fournaise (i.e. topographic effect) ranges between 0 and –3 mV/m (Lénat, 2007). The northeastern crater wall was about 30 m high at the time of the survey, which is too small to explain such a difference of electrical potential by a topographic effect. Moreover, it is interesting to note that along the north-south rift zone axis, five profiles also displays strong SP variations (of several hundreds of mV) between the rim and the floor of Dolomieu crater (see profiles 5, 6, 12, 13 and 14 on figure 3a).

3.2.2- Self-potential zonation inside the Dolomieu crater

242 On Figure 3a the amplitude of the SP signal and the orientation of the isolines
243 highlight a clear zonation between the eastern third and the rest of the Dolomieu crater (also
244 see figure 6). The eastern part of the Dolomieu crater is marked by a nearly E-W SP spatial
245 variation from -1100 mV along the crater wall up to -500 mV near the center of the crater,
246 500 m farther. The isolines show a NNW-SSE orientation while they do not follow a
247 particular direction on the rest of the crater floor. This feature observed on a flat area reflects
248 a clear heterogeneity of the Dolomieu crater structure before the April 2007 collapse.
249
250 3.2.3- Self-potential anomalies around the craters
251
252 On the external edge of the Dolomieu and Bory craters, five small-scale SP maxima
253 are individualized (red-orange color in Fig. 3a, c). These anomalies are located respectively:
254 (1) south of the Dolomieu crater, crossing profiles 16 and 17 (DS in Fig. 3a, c), (2) north of
255 the Dolomieu crater, crossing profile 4 (DNW in Fig. 3a, c), (3) north of the Bory crater,
256 crossing profile 7 (BN in Fig. 3a, c), (4) north of the Dolomieu crater between profile 2 and 3
257 (DN in Fig. 3a, c), (5) south-east of the Dolomieu crater, crossing profile 20 (DE in Fig. 3a,
258 c).
259 (1) In the south, the DS anomaly is 200-250 m wide and globally superposed to the
260 Petit Plateau paleo-pit crater. This later formed around 1791 (Bachèlery, 1981), consists in
261 surface of a system of concentric fractures that delineates the hidden collapsed structure
262 (Peltier et al., submitted). This is one of the areas showing the maximum fracture and fissure
263 density around the Dolomieu crater (see Fig. 5 and Michon et al., 2009a). The related SP
264 maximum has a wider extension than the superficial structural boundary of the Petit plateau
265 pit crater (Fig. 5).

(2) The DNW SP anomaly to the north of Dolomieu (profile 4 on figure 3a, c) corresponds as well to a highly fractured zone. It is related to the hidden boundary of a larger paleo-pit crater named Pre-Bory pit crater (see figure 5; Lénat and Bachèlery, 1990; Michon et al., 2009a). Large part of this SP maximum is located just inside the boundary of Pre-Bory pit crater.

(3) The BN SP anomaly (profiles 7 on figure 3a, c) is located also just inside the Pre-Bory pit crater limits and seems to extend at least up to the northern extremity of profile 6 with a slightly lower SP amplitude.

(4) The DN SP anomaly (between profiles 2 and 3 on figure 3a, c) is located close to the Pre-Bory pit crater but corresponds to another structural boundary named Soufrière pit crater, formed in 1964 (Fig. 5; Carter et al., 2007).

(5) The DE SP anomaly (profile 20 on figure 3a, c) located on the eastern border of Dolomieu, did not appear on the 1981 SP map (Malengreau et al., 1994) but was present in 1992 (Fig. 2: map from Michel and Zlotnicki, 1998) and still exists in 2006 (our survey). Strikingly, several dykes (18-19 December 1975, September 1985, January 1990, July 1991, July 1999 and August 2004 dykes) cross this particular point. Shortly after our survey, the 30 August 2006 eruptive fissure crossed the crater wall at the same point as the December 2003 eruption did before.

Even if the position of the main anomalies in not modified from one survey to the other, by calculating the difference between the 2008 and 2006 SP maps (figure 3d) we can evidence a significant variation of the amplitude of the signal in several areas. We identify an increase of the SP signal at the eastern limit of the northern and southern rift zones and in the southern part of the N120º rift zone, around the Dolomieu crater, (red shades) and a decrease of the signal on the southern rift zone and in part of the northern rift zone (dark blue shades).

4- Discussion: Self Potential as a marker of the structures controlling eruptive and collapse events

The entire cone is characterized by negative self-potential values relative to the sea. The SP distribution depends on the hydrogeological pattern of the study area. Recent studies show that cold and dilute descending groundwater is important for SP generation (Ishido, 2004; Aizawa et al., 2009). Basically, they show that negative SP zones generated by infiltration are the actual anomalies while the SP maxima are created by the surrounding minima. In the case of Piton de la Fournaise, Join et al, (2005) simulation gives hydraulic confirmation of a the presence of a continuous aquifer and of a central groundwater dome. In the Enclos Fouqué Caldera (Fig. 1), the water table is then nearly parallel to the topography (Join et al., 2005). Taking a reference at the sea means we consider the water table is at sea elevation and that the interpretation of SP negative anomalies is downward fluid flow (e.g. see Lénat, 2007). Following the hydrogeological model proposed by Join et al. (2005), in our maps, hydrothermal upwelling will then be marked by SP maxima and positive SP/elevation correlations and infiltration by some SP minima and negative SP/elevation correlations. Moreover, we will interpret the SP data jointly with information from Lénat et al. (2000) on the resistivity structure of the terminal cone and their interpretations in term of hydrothermal activity.

In the typical W-shaped SP signal of active volcanic cones cited before, some authors interpret the two minimums of the W signal as the transition between the hydrogeologic SP signature of the lower flanks (negative SP/elevation correlation) and the hydrothermal SP signature of the upper part of the edifice (positive SP/elevation correlation) (e.g. Zlotnicki et al., 1998; Finizola et al., 2004; Lénat, 2007). Just considering the terminal cone of Piton de la

316 Fournaise volcano, no W-shape signal and very few negative SP/elevation correlations have
317 been observed (Fig. 4). At the scale of the Enclos Fouqué caldera, in the western part, along
318 the SP maximum evidenced by Michel and Zlotnicki (1998) is possibly compatible with a
319 transition to the hydrogeological area but the relationship between SP signal and elevation
320 cannot be established (flat topography in this area). The amplitude of the SP signal on the
321 three main positive SP radial anomalous areas and the positive SP/elevation correlation
322 encountered on all the flanks of the terminal cone, strongly suggest (1) that the whole terminal
323 cone of Piton de la Fournaise is affected by rising of hydrothermal fluids and (2) that the
324 summit craters and the northern, southern, and eastern axes are preferential paths for
325 hydrothermal fluids.
326
327 The strong hydrothermal rising fluids preferentially located in the upper part of the
328 cone and along the three rift zones can hide the presence of infiltration in the surrounding
329 areas. An exception is found along Profile 1 (Fig. 3b) that shows a SP minimum (DNE)
330 associated to a negative SP/elevation gradient (-1.25 mV/m). This suggests that DNE
331 minimum could evidence a preferential downward water flow pathway (Fig. 7).
332
333 The detailed summit SP map and the general SP map of the entire cone of the Piton de
334 la Fournaise volcano offer a good opportunity to discuss the importance of the structural
335 boundaries in controlling hydrothermal fluid flows and potentially magmatic injection. The
336 general SP map shows that the entire edifice is affected by hydrothermal activity, but with
337 different intensities from an area to another.
338 Ishido (2004) demonstrated that, if an electrical conductive structure (as
339 hydrothermally altered rock) extending to deep levels is present below the summit area of a
340 volcanic cone, SP around the summit is substantially increased, resulting in the characteristic

341 strong positive anomaly observed in this area of active volcanoes. Considering the ambiguity
342 in interpreting SP data alone (Revil et al., 2008; Finizola et al., 2006, 2009), it is interesting to
343 compare our SP results and interpretation (see Fig. 7) with the electrical resistivity
344 measurements obtained by Lénat et al., 2000, on the same area, in 1987-1992. The authors led
345 a study of the geoelectrical structure of the central part of Piton de la Fournaise volcano.
346 Beneath the highly active summit area, the authors observed an electrical conductor rising
347 below the terminal cone (resistivity values <20 ohm.m below ~500m depth and <250 ohm.m
348 from ~500m up to ~300 m depth) that they interpreted as an altered hydrothermal zone. The
349 overburden is composed of resistive terrains (1000 to 3000 ohm.m and >8000 ohm.m for the
350 shallowest 100m), typically interpreted as water-sparse region, not significantly affected by
351 hydrothermal circulation (e.g. Aizawa et al., 2009; Garcia and Jones, 2010; Revil et al., 2010).
352 On Piton de la Fournaise, fresh lava flows show resistivity ranging 10000 to 100000 ohm.m
353 so that resistivities of 1000 to 3000 ohm.m can mean a weak hydrothermal circulation.
354 However, areas affected by intensive hydrothermal activity are usually characterized by
355 resistivities ranging from a few ohm.m to few hundreds ohm.m (e.g. Revil et al., 2004, 2008;
356 2011; Finizola et al., 2009, 2010). In our survey performed in July 2006, 9 months before the
357 April 2007 caldera collapse, several evidences attest to an intensification of the hydrothermal
358 activity in the shallower part of the cone below the craters, with respect to the conditions
359 during the 1987-1992 period (Lénat et al., 2000): (1) The sharp SP horizontal gradient (~1000
360 mV in a few tens of meters) between the inner and external part of the Dolomieu crater (Fig.
361 3a) suggests a shallow and strong lateral variation in the fluid circulation pattern and/or in the
362 resistivity structure. (2) Just after the April 2007 collapse, hot areas have been observed on
363 the ground surface through IR camera inside the Dolomieu collapse structure (Staudacher et
364 al., 2010), and (3) hydrothermal alteration has been observed along the cliffs left by the 2007
365 Dolomieu caldera collapse between the surface and 300m depth (Peltier et al., submitted).

366 Because resistivity is highly sensitive to hot and mineralized volcanic fluids like hydrothermal
367 fluids, it is possible that the resistivity structure changed between 1987-1992 and 2006 due to
368 the hydrothermal/magmatic activities (Aizawa et al., 2011, and reference therein). The top
369 300 m beneath Dolomieu crater may have turned to be affected by more intense hydrothermal
370 activity before the 2007 collapse, responsible for the strong SP maxima measured in July
371 2006 in the crater area. Based upon these considerations we can interpret the signal observed
372 on Piton de la Fournaise in terms of spatial variations of underground hydrothermal activity.

373 If some geological and geophysical clues have been found to constrain the shallowest
374 part of the hydrothermal system before the 2007 collapse event, it is not easy to infer the
375 hydrothermal circulation condition at depth from SP data alone. SP sources being broadly
376 distributed in the volcanoes (Yasukawa et al., 2005; Aizawa et al., 2009), the large
377 wavelength (~1 km) superimposed on the northern and southern rift zones (Fig. 5) do not give
378 a strong constrain on the depth of the SP source. Considering the results obtained by Lénat et
379 al., (2000), with resistivity values < 20 ohm.m, up to the maximum depth of investigation
380 (~1000m below the surface), we can reasonably assume that the hydrothermal system is
381 intensively active up to that depth. Below 1000 m depth, we have no data to constrain the
382 hydrothermal fluid flow, as shown on figure 7.

383 Based on our SP study, we highlight the main zones of hydrothermal release of the
384 Piton de la Fournaise and describe various types of structural boundaries:

385 (1) *Summit crater boundaries*: The major structure draining hydrothermal fluids is
386 the Dolomieu-Bory crater zone (Fig. 3). The Dolomieu-Bory boundary is a well-known
387 structural limit. Major part of the dykes associated to summit and proximal eruptions start
388 around this limit (Peltier et al. 2009a). The main SP anomaly then underlines the major rule of
389 this area on the magma transit to the surface on Piton de la Fournaise. The border faults of
390 these two craters (Fig. 5) constitute a major structural barrier reducing drastically the radial

391 diffusion of hydrothermal fluids into the ground, outside the craters. The importance of the
392 Dolomieu-Bory structural boundaries on the control of hydrothermal fluid flow between the
393 inner and the outer part of the Dolomieu-Bory craters is also attested by the data collected
394 after the 5-7th April 2007 Dolomieu caldera collapse. Indeed, the location of the main
395 anomalies on the SP maps of the summit area realized before (July 2006) and after (May
396 2008) the Dolomieu collapse is similar (Fig. 3a and c). This means that this major collapse
397 event did not affect significantly the fluid flow pattern in the vicinity of the collapsed area.
398 This can be easily understood through the geological evolution of the summit area, which has
399 been affected by several collapse and pit-crater events. The most recent ones inside the
400 Dolomieu crater took place between 1931 and 1935 (east), in 1953 (southwest), in 1961
401 (southwest), in 1986 southeast), in 2002 (southwest) and in 2007 (the whole Dolomieu crater)
402 (Peltier et al., 2009b). These events were alternated with periods of eruptive activity refilling
403 the craters through the accumulation of lava flow. The succession of collapse events along the
404 same crater limits (the current Dolomieu-Bory limits) demonstrates the individualization of a
405 rock column delimited by the Dolomieu-Bory boundaries. Such individualization of a rock
406 column explains the localization of the main hydrothermal fluid circulations inside the craters
407 and why the last collapse of April 2007 does not affect significantly the hydrothermal fluid
408 flow pattern. Also, the absence of significant changes in the position of the SP anomalies and
409 the absence of amplitude variation for most part of this area between July 2006 and May 2008
410 (Fig. 3a, c, d) after such a collapse, attests that the pre-existing Dolomieu-Bory structural
411 boundaries were acting as a barrier for lateral fluid flow before the April 2007 collapse.
412 Inside the Dolomieu crater, another structural barrier for fluid flow has been evidenced
413 in the eastern side of the crater. The SP zonation previously described affects the whole
414 Dolomieu crater with a NNW-SSE orientation of the SP isolines on the eastern side of the
415 crater. There was no significant zonation related to the repartition of the recent lava flows and

eruptive vents or fissures on the Dolomieu floor. These considerations make highly improbable the hypothesis of shallow hydrothermal SP sources influencing the observed SP pattern. Rather than a shallow transient anomaly, we think that the SP signal in Dolomieu was revealing a hidden pre-existing fracture or fault system to the east controlling the hydrothermal fluid rising from depth in the crater (Figs. 6 and 7). This hypothesis matches the interpretation proposed by Michon et al. (2009b) on the Dolomieu caldera collapse process. The authors show that the structure of the new Dolomieu caldera and its evolution during the collapse is explained by the collapse of a coherent block limited by vertical to outward dipping fractures at depth and sub-surface normal fractures. According to the first observations, on April 7, 2007, the Dolomieu collapse affected first the western and the northern part of the pre-existing Dolomieu crater while a wide annular plateau corresponding to the pre-existing floor of Dolomieu was remaining in the east (Michon et al., 2007a). On April 10 the caldera was enlarged and only few perched terraces remained from the eastern plateau. The authors add that the similar contours of Dolomieu before the collapse and of the new caldera, remarkably shows the control of the pre-existing structures in the April 2007 caldera collapse. In the same way, we think that the inner structure of the crater controlled the successive phases of the collapse and that the SP signal was marking this particular structure at least 1 year before the collapse. The Dolomieu collapse would result from the combined effect of a progressive destabilization of the rock column above the magma chamber since 2000, and the large amount of magma withdrawal during the early stage of the 2007 eruption (Michon et al., 2007a; Peltier et al., 2009b). The eastern plateau remaining in the first phases of the Dolomieu collapse may be associated to a pre-existing east-dipping fracture individualizing an eastern block in the rock column beneath Dolomieu. The fracture draining hydrothermal fluids, this block may have been relatively isolated from the rest of the crater in terms of fluid advection. This would explain a SP signal progressively decreasing from a

441 hidden fracture to the inner part of the isolated block. Our data matches with a more or less N-
442 S fracture running from the middle-eastern part of Dolomieu at shallow depth to the eastern
443 edge of the crater at depth (Fig. 6).

444 (2) *Pit crater boundaries*: Just outside the Dolomieu and Bory craters, we
445 evidenced thanks to our high resolution map small scale positive anomalies which amplitudes
446 are similar to the highest amplitude inside the Dolomieu and Bory craters. The anomalies of
447 highest amplitude are related with three old pit-crater structures, which are Petit Plateau, Pre-
448 Bory, and Soufrière (see Figs. 5 and 7 for location). In all these cases, the former pit craters
449 cut either the Dolomieu and/or the Bory crater rims. Considering that pit craters are highly
450 fractured zones, they constitute more permeable areas explaining the local rise of
451 hydrothermal fluid flow, of same intensity than inside the Dolomieu and Bory crater. On
452 another hand, the SP anomaly related to the Petit Plateau pit crater being larger than the
453 surface fracture network, a hidden and larger collapse structure could be associated to this
454 structure, at depth (Fig. 5).

455 (3) *Temporally dyke injection pathways*: The only small scale maximum SP
456 anomaly not related with pit crater structure, and already visible in 1992 (Fig. 2) is the south-
457 eastern Dolomieu anomaly (DE on Fig. 3a, c) located on the N120º rift zone and associated to
458 dyke intrusions feeding eruptions close to this area. Three eruptions associated to eruptive
459 fissures and dykes have been crossing recently this site (e.g.: in July 1999, August 2004, and
460 August 2006; Figs. 5 and 7). It is possible that this area was draining hydrothermal fluids
461 along a major structure of the edifice where dykes are preferentially injected. This SP
462 anomaly was already visible on the map made by Michel and Zlotnicki (1998; Fig. 2) in 1992,
463 a few months after the July 1991 eruption and two years after the January 1990 eruption,
464 which occurred both in this area. On the map of 1981 (Malengreau et al., 1994; Fig. 2), no
465 such anomaly is visible revealing that the SP intensity in this area is directly related to dyke

466 emplacement; indeed in 1981 the last dyke injected in this area was in December 1975. So
467 this anomaly can be due to (1) the opening and re-opening of fractures during dyke injections
468 east of the Dolomieu crater which favor temporally deep fluid hydrothermal circulation in this
469 area or to (2) the shallow advection of fluids in the first meters of the ground in recent
470 emplaced lava flows (Barde-Cabusson et al., 2009).

471 (4) *Main rift zone pathways*: Other maximum SP anomaly corresponds to the three
472 main axes pointing to the summit area. The diffuse N110-120º axis corresponds also to a main
473 direction of La Réunion Island associated with the lithospheric structural anisotropy located
474 beneath the island (Michel and Zlotnicki, 1998; Michon et al., 2007b). We can distinguish the
475 main N-S axis, corresponding to the well-known rift zones, and this secondary N110-120º
476 axis of lower intensity. These highly fractured zones are preferential pathways for
477 hydrothermal rising fluids and are thus zones of major permeability and of low mechanical
478 resistance and therefore of major probability of eruption. Indeed, these high permeability
479 areas are preferential pathways for both fluid from the hydrothermal system or for magma
480 rising from depth. On Piton de la Fournaise like in all active hydrothermal fields, the
481 amplitude of the SP anomalies can vary with time (Fig. 2; e.g.; Michel and Zlotnicki, 1998)
482 without changing their spatial distribution, revealing that they are strongly controlled by the
483 structure of the edifice i.e. by the lithological contrasts, the repartition of the fractures and
484 eruptive fissures. It is then not surprising that the preferential hydrothermal circulation
485 underlines the well-known northern and southern rift zones of the volcano (Fig. 2, 3, and 5).
486
487 The rift zones concentrate recent vents, dykes, eruptive fissures and young lava flows
488 (Fig. 5). Since 1998, the activity of Piton de la Fournaise has been characterized by an
489 average of two eruptions per year producing mostly lava flows. As a consequence, the recent
490 (< 10 years) lava overburden is significant on the rift zones. Therefore, the SP positive

491 anomalies can probably be due to (1) transient sources associated to shallow advection of
492 fluids in the first meters of the ground (i.e. recent lava flows; Barde-Cabusson et al., 2009)
493 and (2) deep convection in a hydrothermal system, affecting several hundred meters below the
494 surface (wide-scale convection cells). A denser SP mapping could be compared to the map of
495 the dated lava flows intersecting the rift zones in order to distinguish locally the sources of the
496 SP signal among these two.

497 The SP signal variations between our 2006 and 2008 surveys highlight a strong
498 increase of the signal (more than 350 mV) at the eastern limit of the main N-S rift zone and in
499 the N120º rift zone and a significant decrease (up to -300 mV) on the N-S rift zone itself (Fig.
500 3d). At Piton de La Fournaise, structural analyses and geodetic measurements have shown
501 that the central cone was affected by a preferential eastward motion (Letourneur et al., 2007;
502 Peltier et al., 2009a and references therein). The flank instability can be explained by stress
503 accumulation on the unbuttressed eastern flank due to the successive intrusions and
504 accumulation of magma in the reservoir. The preferential motion of the eastern flank was
505 especially well visible during the large distal eruption of April 2007 (Augier et al., 2008;
506 Peltier et al., 2009b). Interferometric data reveal a motion of up to 80 cm of the eastern flank
507 towards the sea (Augier et al., 2008). The dipolar SP signal observed: increase of the SP
508 signal on the eastern limit of the N-S rift zone and decrease on the N-S rift zone itself can be
509 due to an increase of the permeability along this eastern limit following the large eastward
510 motion of the eastern flank during the April 2007 eruption. The SP decrease observed on the
511 southern rift zone (maximum -300mV) and on part of the northern rift zone (maximum -
512 200 mV on DNW) can evidence an associated balancing of fluid flow circulation in the
513 system. Hydrothermal fluids flow migrated to the more permeable area depleting the fluid
514 supply in the main hydrothermal zones. Interestingly, no significant variation has been
515 measured on the western part of the northern rift zone, on DS and DE. The fluid circulation

516 inside these areas may be isolated from the rest of the system by their own fracture network,
517 explaining why no disruption is observed.
518
519 5. Conclusions
520
521 The SP dataset collected in 2006 allowed us to build a global map of the Piton de la
522 Fournaise's terminal cone and a detailed map of the summit area. We compared it to previous
523 SP maps and confront our results to the geological history of the edifice to make the following
524 conclusions, also synthesized on Figure 7:
525 (1) In addition to the strong SP anomalies characterizing the northern and southern rift zones,
526 the N120º radial anomaly, and the summit area, the entire terminal cone is affected by an
527 extended hydrothermal activity, which prevents from observing a classical W-shape SP signal
528 of an active volcanic cone.
529 (2) The main hydrothermal release has been identified inside the Dolomieu-Bory craters.
530 Their limits are major structural barriers for fluid circulation.
531 (3) The SP mapping in the Dolomieu crater reveals a hidden pre-existing east-dipping fracture
532 or fault system, which controlled the Dolomieu collapse during the April 2007 eruptive crisis
533 of Piton de la Fournaise.
534 (4) As well, the former pit craters surrounding the Dolomieu-Bory craters appear as main
535 fluid paths deeply connected to the central Dolomieu-Bory hydrothermal fluid path. Also the
536 Petit Plateau SP anomaly having a larger extension than the visible associated fractures
537 suggests that the pit crater has a greater extension at depth.
538 (5) The SP increase between 2006 and 2008, along the eastern limit of the N-S rift zone, can
539 be associated to the eastward motion of the eastern flank of the volcano during the April 2007
540 eruption.

SP anomalies can highlight zones of major permeability and of low mechanical resistance, and therefore of major probability of deformation, rupture and/or eruption. Using SP variations to distinguish eruption precursors and low mechanical resistance areas would require a continuous monitoring of the key areas showing the strongest SP anomalies.

Acknowledgments

The field work was supported by The Université de la Réunion (BQR 2005-2006). We are particularly grateful to Benoît Fragnol and Frédéric Lorion for their help in acquiring the SP data in particularly wet and cold conditions. Logistic and field support from Laboratoire GéoSciences Réunion, Observatoire Volcanologique du Piton de La Fournaise, Benoît Welsch, Laurent Michon, Vincent Famin, Nicolas Villeneuve, and Alexandre Nercessian was greatly appreciated. We are grateful to Jean Vandemeulebrouck and Koki Aizawa whose comments helped to substantially improve the manuscript. This is IPGP contribution number 3197.

557 References

558

559 Aizawa, K., 2008. Classification of self-potential anomalies on volcanoes and possible
560 interpretations for their subsurface structure. J. Volcanol. Geotherm. Res. 175(3): 253-
561 268. doi: 10.1016/j.jvolgeores.2008.03.011.

562 Aizawa, K., Uyeshima, M., Nogami, K., 2008. Zeta potential estimation of volcanic rocks on
563 11 island arc-type volcanoes in Japan: implication for the generation of local self-
564 potential anomalies. J. Geophys. Res. 113, B02201. doi:10.1029/2007JB005058.

565 Aizawa, K., Ogawa, Y., Ishido, T., 2009. Groundwater flow and hydrothermal systems within
566 volcanic edifices: Delineation by electric self-potential and magnetotellurics. J.
567 Geophys. Res. - Solid Earth, v. 114.

568 Aizawa, K., Kanda, W., Ogawa, Y., Iguchi, M., Yokoo, A., Yakiwara, H., Sugano, T., 2011.
569 Temporal changes in electrical resistivity at Sakurajima volcano from continuous
570 magnetotelluric observations. J. Volcanol. Geotherm. Res., 199(1-2): 165-175. doi:
571 10.1016/j.jvolgeores.2010.11.003.

572 Augier, A., Froger, J.L., Cayol, V., Fukushima, Y., Tinard, P., Souriot, T., Mora, O.,
573 Staudacher, T., Durand, P., Fruneau, B., Villeneuve, N., 2008. The April 2007
574 eruption at Piton de la Fournaise, Réunion Island, imaged with ENVISAT-ASAR and
575 ALOS-PALSAR data, USEReST worhshop, Napoli, Italy.

576 Bachèlery, P., 1981. Le Piton de la Fournaise (Ile de la Réunion). Etude volcanologique,
577 structurale et pétrologique. PhD thesis, Univ. Clermont-Ferrand II, 215 pp.

578 Barde-Cabusson, S., Levieux, G., Lénat, J.-F., Finizola, A., Revil, A., Chaput, M., Dumont,
579 S., Duputel, Z., Guy, A., Mathieu, L., Saumet, S., Sorbadère, F., Vieille, M., 2009.
580 Transient self-potential anomalies associated with recent lava flows at Piton de la

581 Fournaise volcano (Réunion Island, Indian Ocean). J. Volcanol. Geoth. Res. 187,
582 p.158–166. doi:10.1016/j.jvolgeores.2009.09.003.
583 Bedrosian, P. A., Unsworth, M. J., Johnston, M. J. S., 2007. Hydrothermal circulation at
584 Mount St. Helens determined by self-potential measurements. J. Volcanol. Geotherm.
585 Res. 160, 137– 146.
586 Boubekraoui, S., Aubert, M., 1999. Apport de la méthode des potentiels spontanés à la
587 reconnaissance géologique et hydrogéologique des terrains volcaniques superficiels du
588 Grand-Brûlé (Réunion, Océan Indien). Hydrogéologie 1: 43-51.
589 Carter, A., van Wyk de Vries, B., Kelfoun, K., Bachèlery, P., Briole, P., 2007. Pits, rifts and
590 slumps: the summit structure of Piton de la Fournaise. Bull. Volcanol. 69, 741-756.
591 doi: 10.1007/s00445-006-0103-4.
592 Corwin, R.F., 1997. The self-potential method for environmental and engineering
593 applications: geotechnical and environmental geophysics. In: Ward, H. (Ed.),
594 Investigations in Geophysics: Soc. Expl. Geophys. vol. 5, p. 1.
595 Finizola, A., Lénat, J.-F., Macedo, O., Ramos, D., Thouret, J.-C., Sortino, F., 2004. Fluid
596 circulation and structural discontinuities inside Misti volcano (Peru) inferred from self-
597 potential measurements. J. Volcanol. Geotherm. Res. 135, 343–360.
598 Finizola, A., Revil, A., Rizzo, E., Piscitelli, S., Ricci, T., Morin, J., Angeletti, B., Mocochain,
599 L., Sortino, F., 2006. Hydrogeological insights at Stromboli volcano (Italy) from
600 geoelectrical, temperature, and CO2 soil degassing investigations. Geophys. Res. Lett.
601 33, L17304. doi:10.1029/2006GL026842.
602 Finizola, A., Aubert, M., Revil, A., Schütze, C., Sortino, F., 2009. Importance of structural
603 history in the summit area of Stromboli during the 2002–2003 eruptive crisis inferred
604 from temperature, soil CO_2, self-potential, and electrical resistivity tomography. J.
605 Volcanol. Geotherm. Res. 183, 213–227. doi:10.1016/j.jvolgeores.2009.04.002.

606 Finizola, A., Ricci, T., Deiana, R., Barde-Cabusson, S., Rossi, M., Praticelli, N., Giocoli, A.,
607 Romano, G., Delcher, E., Suski, B., Revil, A., Menny, P., Di Gangi, F., Letort, J.,
608 Peltier, A., Villasante-Marcos, V., Douillet, G., Avard, G., Lelli, M., 2010. Adventive
609 hydrothermal circulation on Stromboli volcano (Aeolian Islands, Italy) revealed by
610 geophysical and geochemical approaches: Implications for general fluid flow models on
611 volcanoes. J. Volcanol. Geotherm. Res. 196, 111-119.
612 doi:10.1016/j.jvolgeores.2010.07.022.
613 Garcia, X., Jones, A.G., 2010. Internal structure of the western flank of the Cumbre Vieja
614 volcano, La Palma, Canary Islands, from land magnetotelluric imaging. J. Geophys.
615 Res.,-Solid Earth 115: 12 B07104. doi:10.1029/2009jb006445.
616 Guichet, X., Zuddas, P., 2003. Effect of secondary minerals on electrokinetic phenomena
617 during water-rock interaction. Geophys. Res. Lett., 30(13), 1714.
618 doi:10.1029/2003GL017480.
619 Hase, H., Ishido, T., Takakura, S., Hashimoto, T., Sato, K., Tanaka, Y., 2003. ζ potential
620 measurement of volcanic rocks from Aso caldera. Geophys. Res. Lett. 30 (23), 2210.
621 doi:10.1029/2003GL018694.
622 Ishido, T., 2004. Electrokinetic mechanism for the ‘‘W’’-shaped self-potential profile on
623 volcanoes. Geophys. Res. Lett. 31: L15616. doi:10.1029/2004GL020409.
624 Ishido, T., Kiruchi, T., Matsushima, N., Yano, Y., Nakao, S., Sugihara, M., Tosha, T.,
625 Takakura, S., Ogawa, Y., 1997. Repeated self potential profiling of Izu-Oshima
626 Volcano, Japan. J. Geomagn. Geoelectr. 49, 1267–1278.
627 Join, J.-L., Folio, J.-L., Robineau, B., 2005. Aquifers and groundwater within active shield
628 volcanoes. Evolution of conceptual models in the Piton de la Fournaise volcano. J.
629 Volcanol. Geotherm. Res. 147, 187-201. doi:10.1016/j.jvolgeores.2005.03.013.

630 Labazuy, P., Saracco, G., Lénat, J.-F., Charbonnier, S., Mauri, G., 2004. EM tomography and
631 modeling of the hydrothermal system of Piton de la Fournaise, Reunion Island.
632 IAVCEI 2004 General Assembly, Pucón, Chile, s08e_pf_142.
633 Lénat, J.-F., 1987. Structure et Dynamique internes d'un volcan basaltique intraplaque
634 océanique: Le Piton de la Fournaise (Ile de la Réunion). PhD thesis, Université Blaise
635 Pascal, Clermont-Ferrand, France.
636 Lénat, J.-F., 2007. Retrieving self-potential anomalies in a complex volcanic environment: an
637 SP/elevation gradient approach. Near Surf. Geophys. 5, 161–170.
638 Lénat, J.-F., Bachèlery, P., 1990. Structure et fonctionnement de la zone centrale du Piton de
639 la Fournaise. Dans : J.-F. Lénat (Ed.), Le volcanisme de la Réunion – Monographie.
640 Cent. Rech. Volcanol., Clermont-Ferrand, France, 257-296.
641 Lénat, J.F., Fitterman, D., Jackson, D. B., Labazuy, P., 2000. Geoelectrical structure of the
642 central zone of Piton de la Fournaise volcano (Réunion). Bull. Volcanol. 62:75–89.
643 Levieux, G., 2004. Construction d'une carte régionale de polarisation spontanée au Piton de la
644 Fournaise. Analyse des anomalies. Mémoire de Travail d'Étude et de Recherche de
645 Maîtrise Thesis, Université Blaise Pascal, Clermont-Ferrand, France, 64 pp.
646 Linde, N., Jougnot, D., Revil, A., Matthaï, S.K., Arora, T., Renard, D., Doussan, C., 2007.
647 Streaming current generation in two-phase flow conditions. Geophys. Res. Lett. 34
648 (3), L03306. doi:10.1029/2006GL028878.
649 Malengreau, B, Lénat, J.-F., Bonneville, A., 1994. Cartographie et surveillance temporelle des
650 anomalies de Polarisation Spontanée (PS) sur le Piton de la Fournaise. Bull Soc Géol.
651 France 165, 221–232.
652 Massenet, F., Pham, V. N., 1985. Experimental and theoretical basis of self-potential
653 phenomena in volcanic areas with reference to results obtained on Mount Etna
654 (Sicily). Earth Planet. Sci. Lett. 73, 415–429.

655 Michel, S., Zlotnicki, J., 1998. Self-potential and magnetic surveying of la Fournaise volcano
656 (Réunion Island): Correlations with faulting, fluid circulation and eruption. J.
657 Geophys. Res. 103, NO B8, 17,845-17,857.
658 Michon, L., Staudacher, Th., Ferrazzini, V., Bachèlery, P., Marti, J., 2007a. April 2007
659 collapse of Piton de la Fournaise: a new example of caldera formation. Geophys. Res.
660 Lett. 34, L21301. doi:10.1029/2007GL031248.
661 Michon, L., Saint-Ange, F., Bachèlery, P., Villeneuve, N., Staudacher, Th., 2007b. Role of
662 the structural inheritance of the oceanic lithosphere in the magmato-tectonic evolution
663 of Piton de la Fournaise volcano (La Réunion Island). J. Geophys. 112, B04205.
664 doi:10.1029/2006JB004598.
665 Michon, L., Cayol, V., Letourneur, L., Peltier, A., Villeneuve, N., Staudacher, T., 2009a.
666 Edifice growth, deformation and rift zone development in basaltic setting: insights
667 from Piton de la Fournaise shield volcano (Reunion Island). J. Volcanol. Geotherm.
668 Res. 184 (1-2), p. 14-30. doi:10.1016/j.jvolgeores.2008.11.002.
669 Michon, L., Villeneuve, N., Catry, Th., Merle, O., 2009b. How summit calderas collapse on
670 basaltic volcanoes: new insights from the April 2007 caldera collapse of Piton de la
671 Fournaise volcano. J. Volcanol. Geotherm. Res. 184 (1-2), 138-151.
672 doi:10.1016/j.jvolgeores.2008.11.003.
673 Nourbehecht, B., 1963. Irreversible thermodynamic effects in inhomogeneous media and their
674 applications in certain geoelectric problems. Ph.D. Thesis, Mass. Inst. Of Technology,
675 Cambridge.
676 Overbeek, J.T.G., 1952. Electrochemistry of the double layer. In: Kruyt, H.R. (Ed.), Colloid
677 Science. : Irreversible Systems, vol. 1. Elsevier Sci, New York, pp. 115–193.
678 Peltier, A., Massin, F., Bachèlery, P., Finizola, A.. Submitted. Lithostratigraphy and
679 volcanological history of the terminal cone of Piton de La Fournaise volcano (La

680 Réunion Island): a review from new field investigations and historical reports, J.
681 Volcanol. Geotherm. Res.
682 Peltier, A., Bachèlery, P., Staudacher, T., 2009a. Magma transport and storage at Piton de La
683 Fournaise (La Réunion Island) between 1972 and 2007: a review of geophysical and
684 geochemical data. J. Volcano. Geotherm. Res. 184(1-2), 93-108.
685 Peltier, A., Staudacher, T., Bachèlery, P., Cayol, V., 2009b. Formation of the April 2007
686 caldera collapse at Piton de La Fournaise volcano: insights from GPS data, J. Volcano.
687 Geotherm. Res. 184 (1-2), 152-163.
688 Revil, A., 2002. Comment on "Rapid fluid disruption: a source for self-potential anomalies on
689 volcanoesa" by M. J. S. Johnston, J. D. Byerlee, and D. Lockner. J. Geophys. Res. 107
690 (B8). doi:10.1029/2001JB000788.
691 Revil, A., Cerepi, A., 2004. Streaming potential in two-phase flow condition. Geophys. Res.
692 Lett. 31 (11), L11605. doi:1029/2004GL020140, 2004.
693 Revil, A., Saracco, G., Labazuy, P., 2003. The volcano-electric effect. J. Geophys. Res. 108,
694 B5, 10.1029/2002JB001835.
695 Revil, A., Johnson, T.C., Finizola, A., 2010. Three-dimensional resistivity tomography of
696 Vulcan's forge, Vulcano Island, southern Italy. Geophys. Res. Lett. 37, L15308. doi:
697 10.1029/2010gl043983.
698 Revil, A., Finizola, A., Sortino, F., Ripepe, M., 2004. Geophysical investigations at Stromboli
699 volcano, Italy. Implications for ground water flow and paroxysmal activity. Geophys.
700 J. Int. 157, 426-440. doi:10.1111/j.1365-246X.2004.02181.x
701 Revil, A., Finizola, A., Piscitelli, S., Rizzo, E., Ricci, T., Crespy, A., Angeletti, B., Balasco,
702 M., Barde Cabusson, S., Bennati, L., Bolève, A., Byrdina, S., Carzaniga, N., Di Gangi,
703 F., Morin, J., Perrone, A., Rossi, M., Roulleau, E., Suski, B., 2008. Inner structure of
704 La Fossa di Vulcano (Vulcano Island, southern Tyrrhenian Sea, Italy) revealed by high

resolution electric resistivity tomography coupled with self-potential, temperature, and CO_2 diffuse degassing measurements. J. Geophys. Res. 113, B07207. doi:10.1029/2007JB005394

Revil, A., Finizola, A., Ricci, T., Delcher, E., Peltier, A., Barde-Cabusson, S., Avard, G., Bailly, T., Bennati, L., Byrdina, S., Colonge, J., Di Gangi, F., Douillet, G., Lupi, M., Letort, J., Tsang Hin Sun, E., 2011. Hydrogeology of Stromboli volcano, Aeolian Islands (Italy) from the interpretation of resistivity tomograms, self-potential, soil temperature, and soil CO_2 concentration measurements. Geophys. J. Int. 186, 1078-1094. doi: 10.1111/j.1365-246X.2011.05112.x

Sill, W. R., 1983. Self potential modeling from primary flows. Geophysics, v. 48, pp. 76-86.

Staudacher, T., 2010. Field observations of the 2008 summit eruption at Piton de la Fournaise (Ile de La Réunion) and implications for the 2007 Dolomieu collapse. J Volcanol Geotherm Res 191, 60-68.

Urai, M., Geshi, N., Staudacher, T., 2007. Size and volume evaluation of the caldera collapse on Piton de la Fournaise volcano during the April 2007 eruption using ASTER stereo imagery. Geophys. Res. Lett. L22318. doi:10.1029/2007GL031551.

Yasukawa, K., Ishido, T., Suzuki, I., 2005. Geothermal reservoir monitoring by continuous self-potential measurements, Mori geothermal field, Japan. Geothermics 34(5): 551-567. doi: 10.1016/j.geothermics.2005.04.005.

Zlotnicki, J., Michel, S., Annen, C., 1994. Anomalies de polarisation spontanée et systèmes convectifs sur le volcan du Piton de la Fournaise (Ile de Réunion, France). C R Acad Sci Paris Sci Terre Planètes (Earth Planet Sci) 318, 1325–1331.

Zlotnicki, J., Boudon, G., Viode, J.P., Delarue, J.F., Mille, A., and Bruere, F., 1998. Hydrothermal circulation beneath Mount Pelee inferred by self potential surveying. Structural and tectonic implications. J. Volcanol. Geotherm. Res. 84, 73-91.

731 Figure Captions

732

733 Figure 1. Overview of the main features of La Réunion Island discussed in the text. B: Bory
734 crater; D: Dolomieu crater; NRZ and SRZ: northern and southern Rift Zones.

735

736 Figure 2. Self potential maps obtained in 1981 and 1992-93. White dotted lines correspond to
737 the location of the measured points (variable spacing).

738

739 Figure 3. (a) Self potential maps of the summit area of the Piton de la Fournaise in 2006, and
740 (c) 2008, (d) difference between them, and (b) self potential map of the terminal cone in 2006.
741 BN stands for Bory north, DNW for Dolomieu north-west, DN for Dolomieu north, DNE for
742 Dolomieu north-east, DE for Dolomieu east, DS for Dolomieu south. White dots are the
743 measured points, black numbers refer to the profiles, and the black arrow points at the
744 measured point used to connect our dataset to a previous one (Levieux, 2004 and Lénat, 2007)
745 in order to reference our maps to the sea (see text).

746

747 Figure 4. Plot of elevation versus SP for the 2006 dataset of Piton de la Fournaise. Note the
748 globally positive correlation between SP and elevation over the whole dataset. The global
749 gradient was estimated graphically, plotting the corresponding trendlines for the flanks of the
750 cone and for the summit area (profiles surrounding the craters) data. The value for each
751 profile has also been estimated to give a range of the values encountered (see text).

752

753 Figure 5: Distribution of the eruptive fissures visible in the field (thin black line, after Michon
754 et al., 2009a). Light blue lines are eruptive fissures from 1998 to 2007 (Peltier et al., 2009a).
755 The bold black lines are the estimated dyke location associated to proximal eruptions between

1981 and 2006 from Michon et al. (2009a). PB stands for Pre-Bory pit crater, S for Soufrière pit crater, and PP for Petit Plateau pit crater. Dark blue lines are the major structural limits influencing SP measurements (see text).

Figure 6. (a) Photo taken on the 6th April 2007 (courtesy of "Gendarmerie nationale") from Bory crater, looking at the east and (b) its interpretation; red shapes correspond to fresh lava flows emitted during the 30 August 2006 - 1 January 2007 eruption, and not yet cold in subsurface in April 2007. (c) On the eastern side of the Dolomieu crater, our 2006 SP map shows a pattern that can be interpreted as the control of the hydrothermal circulation by a pre-existing fault inside Dolomieu (white strokes). In 2007 this structure led to the formation of the eastern plateau during one stage of the Dolomieu caldera collapse. (d) Schematic structural map from Michon et al., 2007a.

Figure 7. Synthetic map (left) and 3-D block (right) of the main features evidenced by the self potential signal and of our main conclusions. In the synthetic map, N10º, N25º, and N110-120º refer to the direction of the rift zones (light-grey areas). The red points refer to the five SP maximum evidenced around Dolomieu and Bory craters. In the 3-D block, the black arrows highlight the main structural limits involved in the Dolomieu April 2007 collapse; the red arrows represent rising hydrothermal fluids. Hydrothermal circulation at depth is constrained up to 1000 m below the topography using electrical resistivity data from Lénat et al. (2000). The blue arrows represent infiltration and lateral cold groundwater flow (water table) as proposed by Join et al., (2005).

Figure 1

Click here to download high resolution image

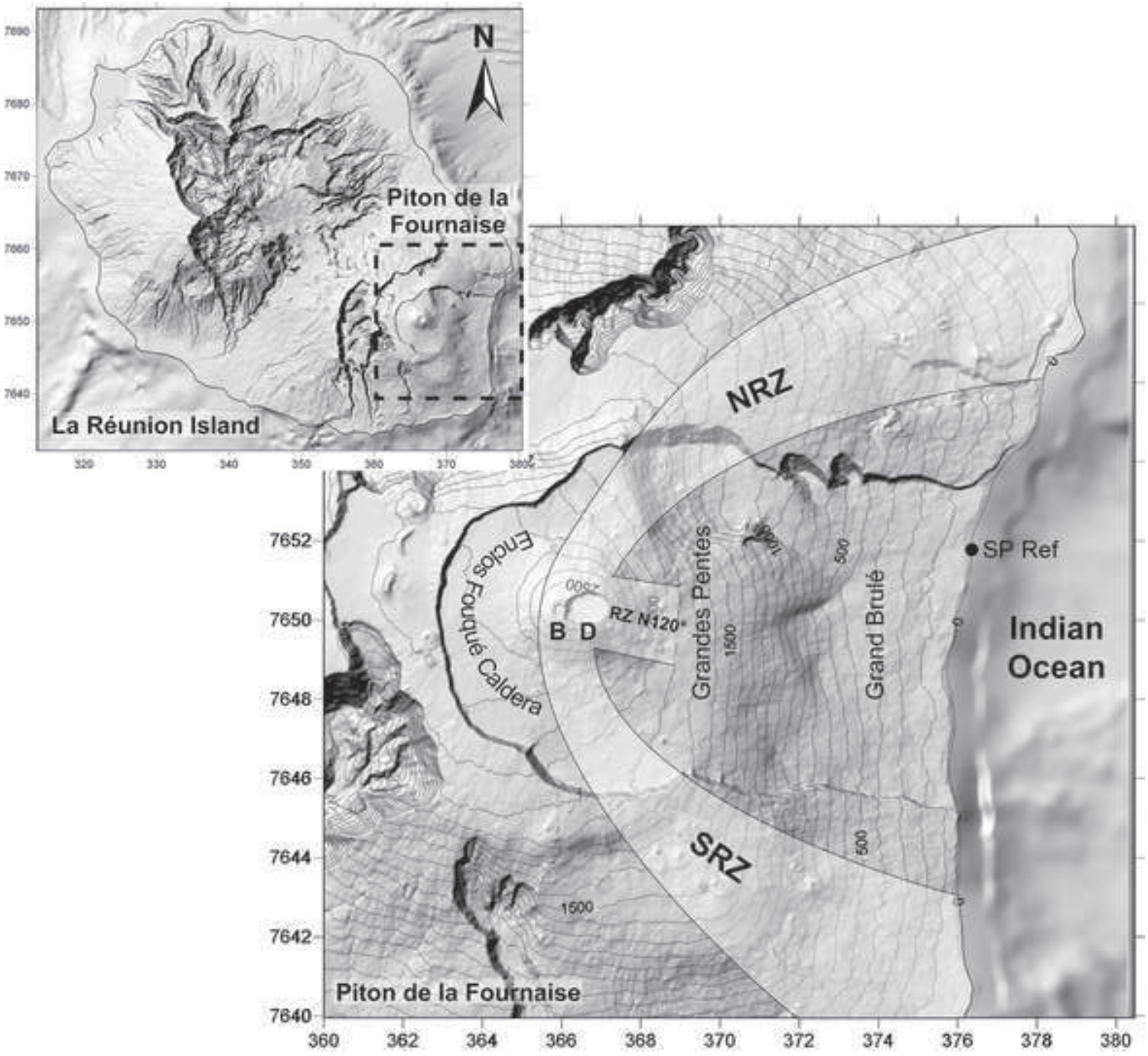

Figure 2
Click here to download high resolution image

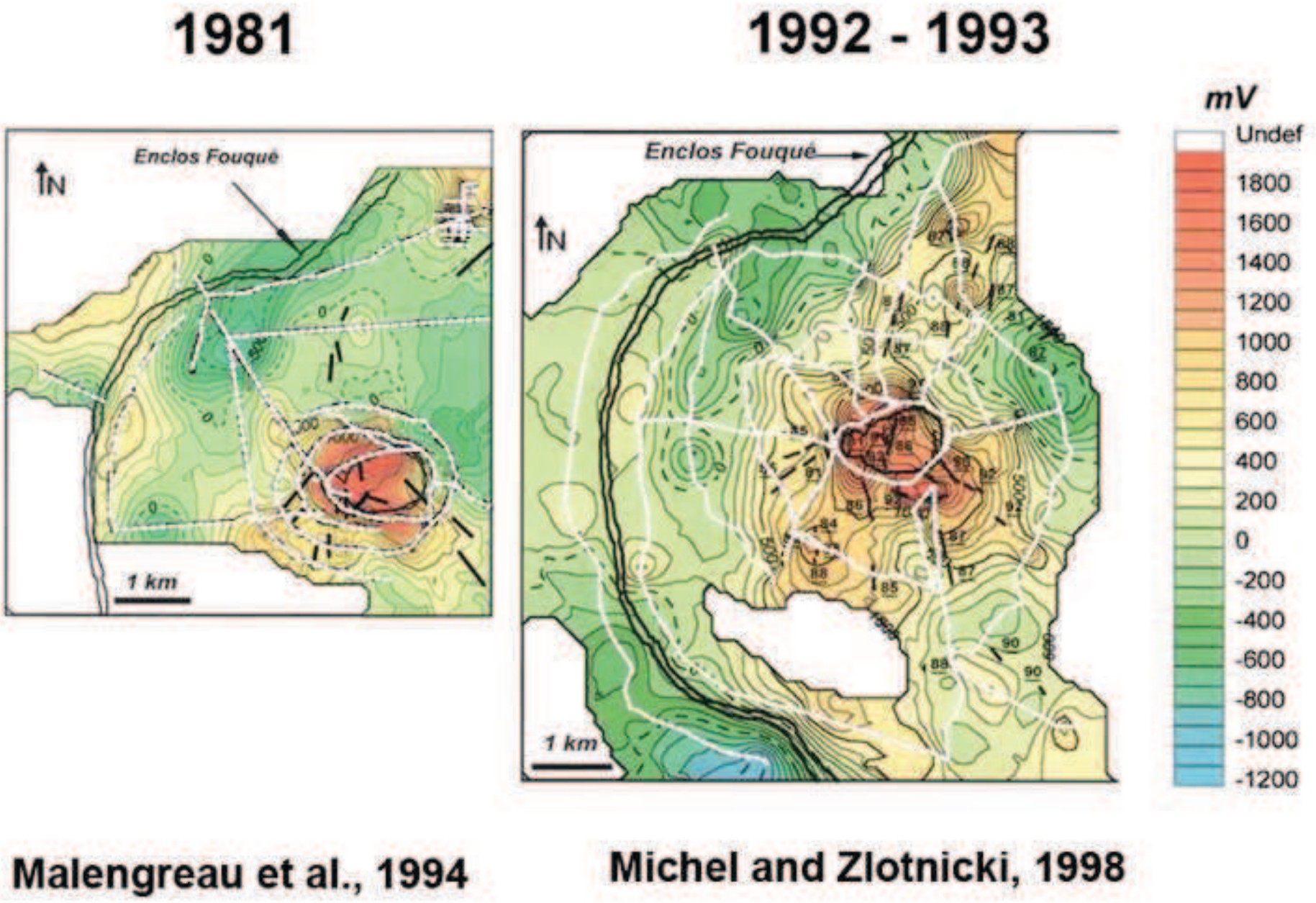

Figure 3

Click here to download high resolution image

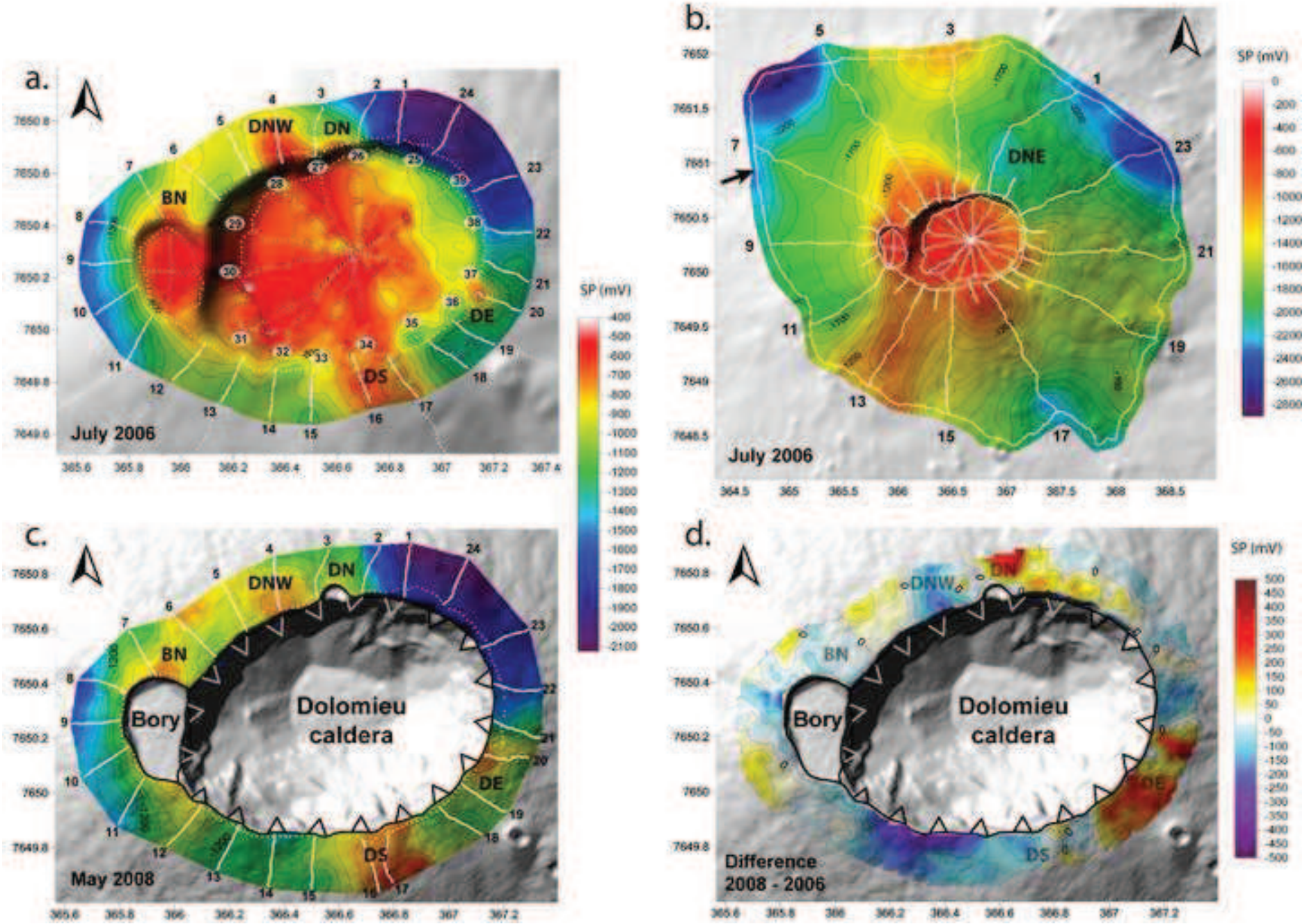

Figure 4
Click here to download high resolution image

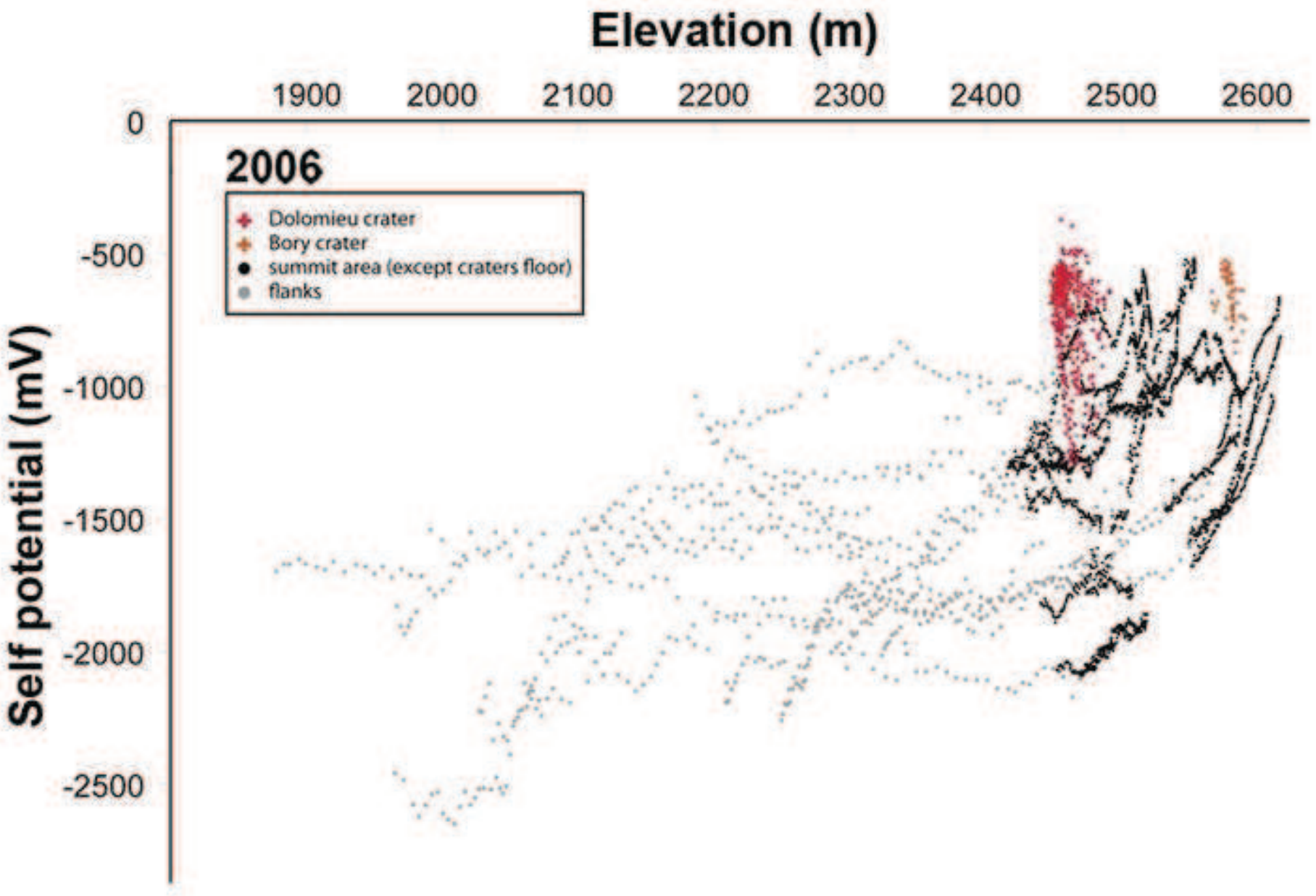

Figure 5

Click here to download high resolution image

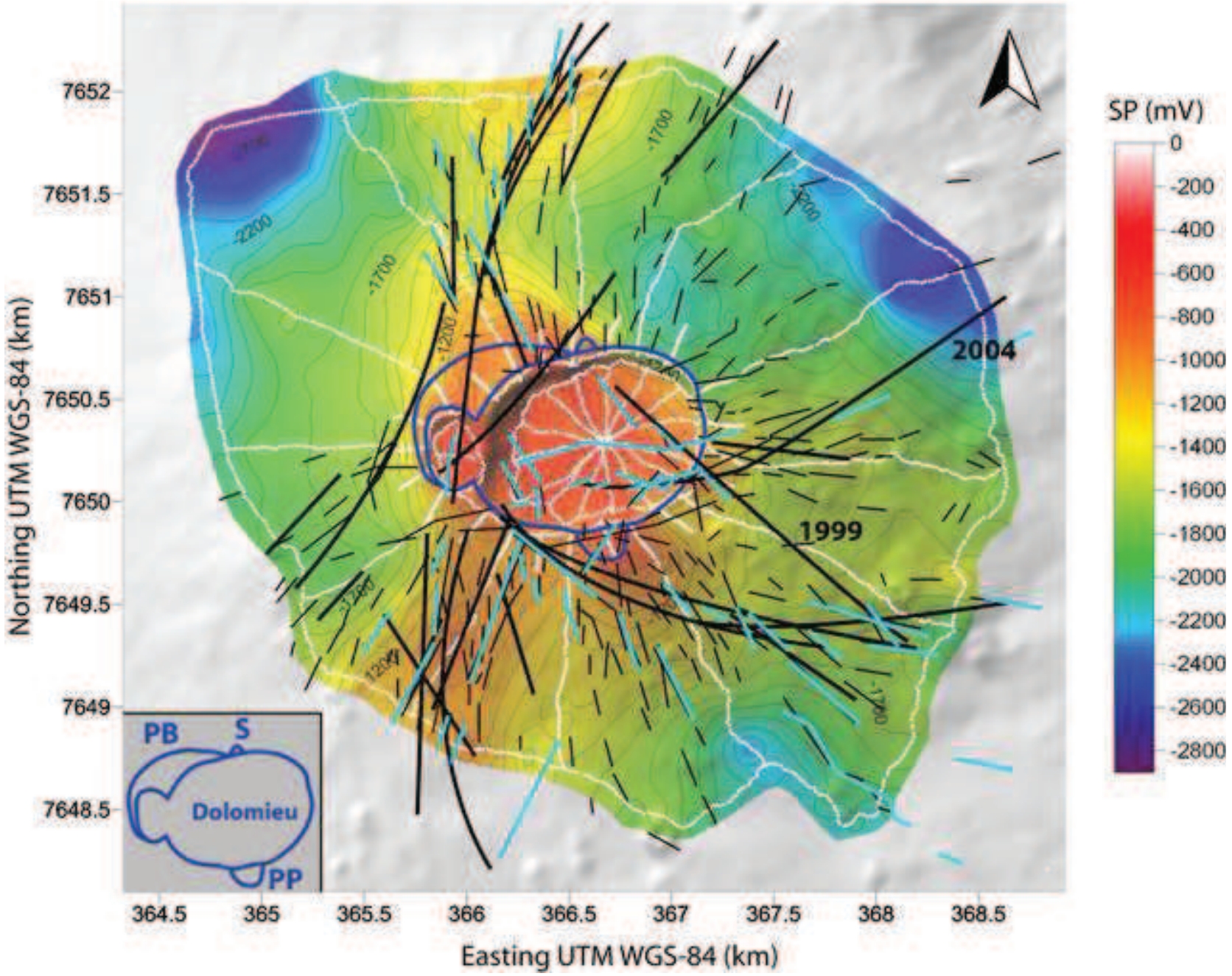

Figure 6

Click here to download high resolution image

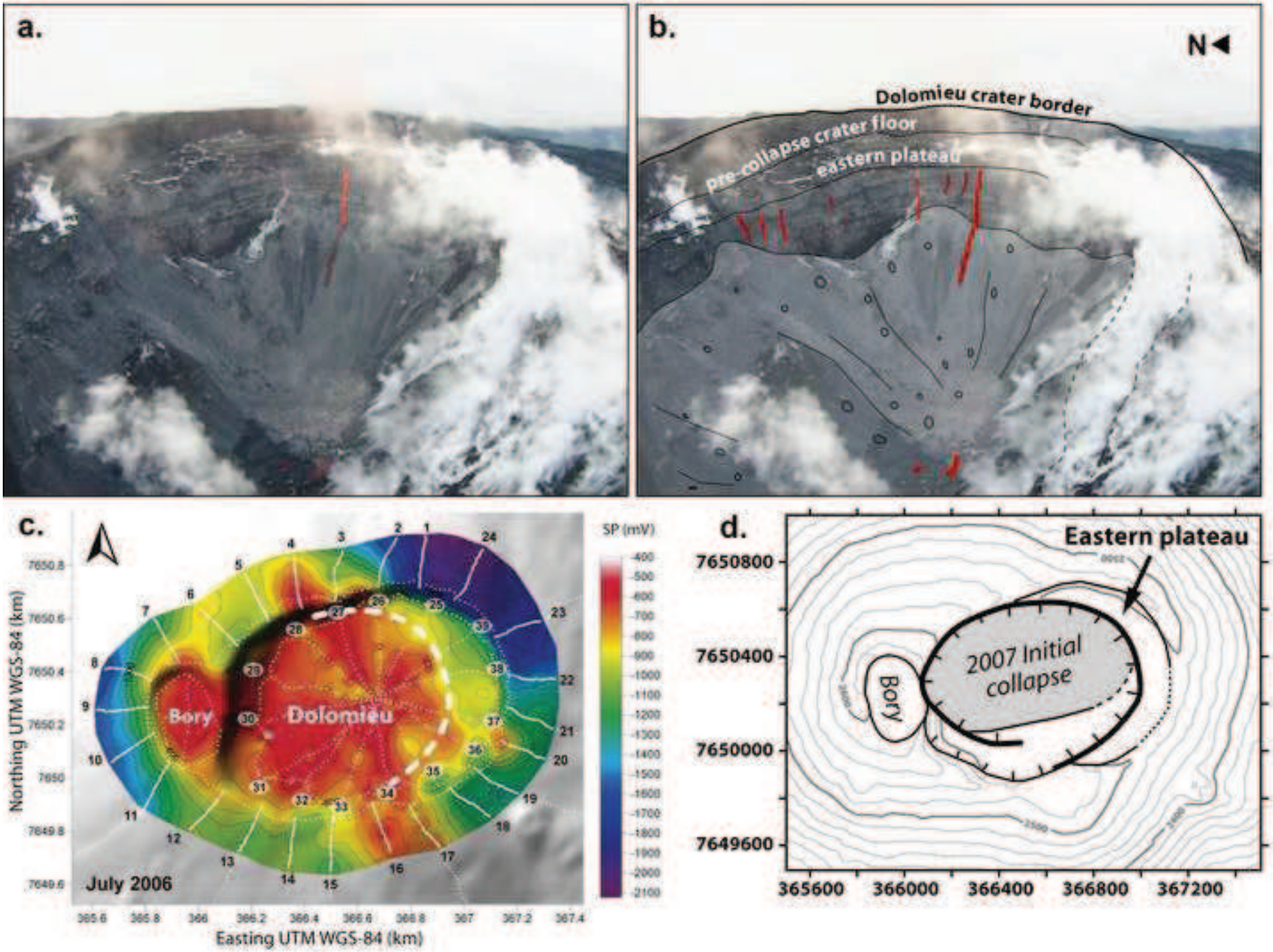

Figure 7

Click here to download high resolution image